The European XFEL Project

Ulrich Trunk

Photon-Science Detector Group,
Deutsches Elektronen-Synchrotron DESY, Hamburg, Germany
ulrich.trunk@desy.de

Abstract

The European XFEL project is a 4^{th} generation photon source to be built in Hamburg. Electron bunches, accelerated to 17.5 GeV by the XFEL linac, are distributed to three long SASE undulators. There photon pulses with full lateral coherence and wavelengths between 0.1 nm and 4.9 nm (12.4 keV and 0.8 keV) are generated for three beamlines. It will deliver around 10^{12}photons within each 100 fs pulse, reaching a peak brilliance of $10^{33}\text{photonss}^{-1}\text{mm}^{-2}\text{mrad}^{-2}(0.1\%\text{BW})^{-1}$. Thus it will offer unprecedented possibilities in photon science research including nano-object imaging and studies (e.g. by coherent X-ray scattering) and ultra fast dynamic analysis of plasma and chemical reactions (e.g. by X-ray photo correlation spectroscopy). The detector requirements for such studies are extremely challenging: position sensitive area detectors have to provide a dynamic range of $\geq 10^4$, with single-photon sensitivity, while withstanding radiation doses up to 1 GGy (TID). Furthermore the detectors have to record data from *trains* of up to 3000 photon pulses, delivered at 5 MHz, which repeat every 100 ms. Three consortia have picked up the challenge to build pixel detectors for the European XFEL DEPFET-APS, AGIPD[1] and LPD. Besides the European XFEL source and the related experimental techniques, the concepts and specialities of the DEPFET-APS, AGIPD and LPD detectors are discussed.

I. Introduction

The application of ulta-short pulses of coherent, visible light generated by lasers provided many fields of research with new insights and discoveries. Detailed investigations on the dynamics of chemical reactions and on the structure of materials can serve as classical examples. Shorter wavelengths, in the regime from VUV to hard X-rays, on the other hand permit the investigation of even smaller structures. But even when created in synchrotrons, the three key features of advanced laser light sources – coherence, ultra short pulselength and power – were not available before the discovery of the SASE[2] principle of free electron lasers. However, the length of SASE undulators and the repeated perturbation of the electron beam induced by the random photon-emission process in a storage ring put up a lower limit to the phase space of the electrons in the magnetic lattice. The solution to overcome this limitation and thus further improve brilliance and coherence of the radiation is the employment of a *single pass* electron source, i.e. a linear accelerator. The TESLA[3] technology developed at DESY for the ILC would make up an ideal electron source to drive such a SASE FEL. So it comes to no surprise that already the TTF1 and TTF2[4] accelerators were coupled to SASE undulators. The latter was renamed to FLASH[5] when it went into user operation in 2005 as the first VUV FEL source. In turn the intriguing idea of using Tesla/ILC to deliver electrons for an FEL emerged. The performance of this source would be unprecedented and open the doors for new areas in photon science.

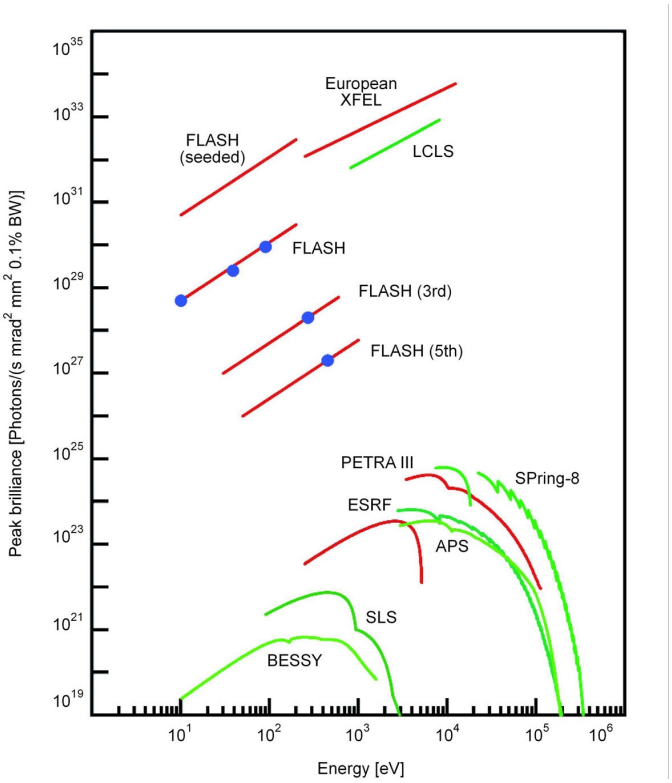

Figure 1: Peak brilliance of current and projected synchrotron radiation sources.

The obvious scientific benefit, the uncertainty about the construction of the future ILC and the availability of technology, know-how and experience at DESY led to the proposal of the European XFEL project in 2003 as a *stand-alone* facility. It is set up as a limited liability company (XFEL GmbH), receiving funding from 12 European countries plus China and Russia. The scientific potential is also unprecedented, exceeding existing 3^{rd} generation synchrotron sources in coherence and brilliance by

[1] Originally presented as Hybrid Pixel Array Detector (HPAD) but renamed to AGIPD for uniqueness.
[2] Self-Amplified Spontaneous Emission
[3] TeV Superconducting Linear Accelerator
[4] Tesla Test Facility
[5] Free electron LASer in Hamburg

several orders of magnitude. Fig. 1 shows the peak brilliance of the European XFEL in comparison to other 3^{rd} generation sources, which it surpasses by a factor $\approx 10^9$. Also in average brilliance it exceeds existing 3^{rd} generation sources by a factor of $\approx 10^5$.

II. The European XFEL Source

The European XFEL source consists of two parts: A 20 GeV electron linear accelerator and three electron beamlines with SASE undulator magnets. Both parts are mounted in a 3.4 km long tunnel, 12 m to 44 m underground. It leads from the premises of Deutsches Elektronrnsynchrotron (DESY) in Hamburg-Bahrenfeld to the experimental site in Schenefeld, Pinneberg district, in the state of Schleswig-Holstein, as shown in fig. 2.

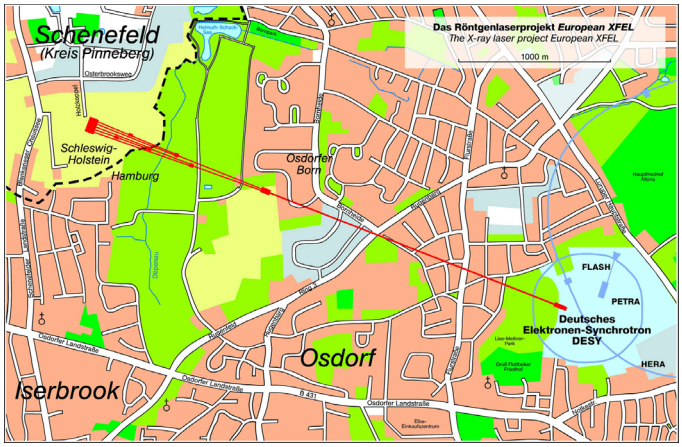

Figure 2: Geographical map of the European XFEL civil construction.

A. The Electron Accelerator

The electron accelerator's beam is generated in an laser-driven photocathode RF gun, located in the injector building on the DESY site in Hamburg-Bahrenfeld. The electrons are then transferred to the main accelerator tunnel, where these enter the first acceleration unit consisting of four superconducting accelerator modules, which in turn contain eight RF cavities made of pure niobium each. The modules operate in the L-band (1.3 GHz) with four modules driven by one RF station. Having passed the first module, the electrons of 0.5 Gev pass a 3^{rd} harmonic RF-system to adjust the longitudinal phase space conditions and a magnetic bunch compressor. After passing three more superconducting accelerator modules and a second bunch compressor, the electron bunches have reached 2 Gev/e and a peak current of 500 kA, which is 100 times higher than the original peak current provided by the injector. The final acceleration to the maximum beam energy of 20 GeV is accomplished in the main part of the linac – 100 superconducting accelerator modules driven by 25 RF stations. The following conventional electron beamline is equipped with collimation and feedback devices, the latter used for trajectory feedback and transfers the electron bunches to the beam distribution system, which mainly consists of two kicker magnets: a *fast kicker* to remove "bad" bunches and to mask the switching transition of the (slow) *flat-top kicker*. The latter is used to switch the electron beam between the SASE2 and the (combined) SASE1/SASE3 electron beamlines. The following list summarises the key parameters of the electron linac, while fig. 3 shows the schematic layout of the accelerator.

- $W_{\mathrm{max}} = 17.5\mathrm{GeV}(20\mathrm{GeV})$
- $I_{\mathrm{peak}} = 5\mathrm{kA}$
- $Q_{\mathrm{bunch}} = 1\mathrm{nC}$
- $P_{\mathrm{beam}} = 600\mathrm{kW}$
- $N_{\mathrm{bunch}} = 3000(3250)$
- $E_{\mathrm{acc}} = 23.6\mathrm{MV/m}$
- $f_{\mathrm{bunch}} = 5\mathrm{MHz}$
- $f_{\mathrm{cycle}} = 10\mathrm{Hz}$
- 29 RF stations
- 928 cavities
- 116 modules
- $P_{\mathrm{RF}} = 5.2\mathrm{MW}$
- Emittance (@ undulator) $= 1.4\,\mathrm{mm} \times \mathrm{mrad}$
- $\Delta E(@\mathrm{undulator}) = 1\,\mathrm{MeV}$
- 2 bunch compressors:
  - $1/20@0.5\,\mathrm{GeV}$
  - $1/5@2.0\,\mathrm{GeV}$

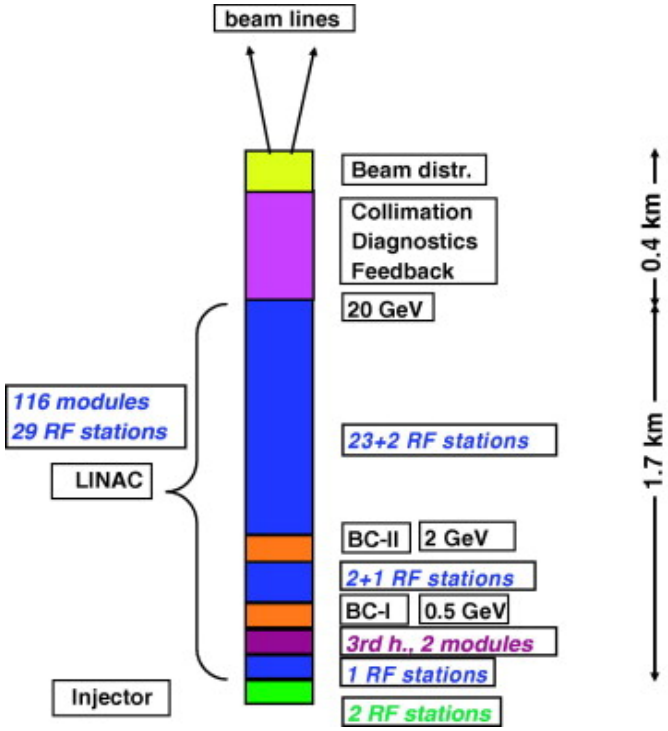

Figure 3: Schematic layout of the European XFEL accelerator.

The relatively strange bunch structure depicted in fig 4 is a compromise of incompatible reqirements:

- highest electron density possible for maximum FEL pulse intensity
- permissible heat load of the superconducting cavities ($\leq$ 3000 full bunches/s)
- minimum bunch spacing for trajectory feedback

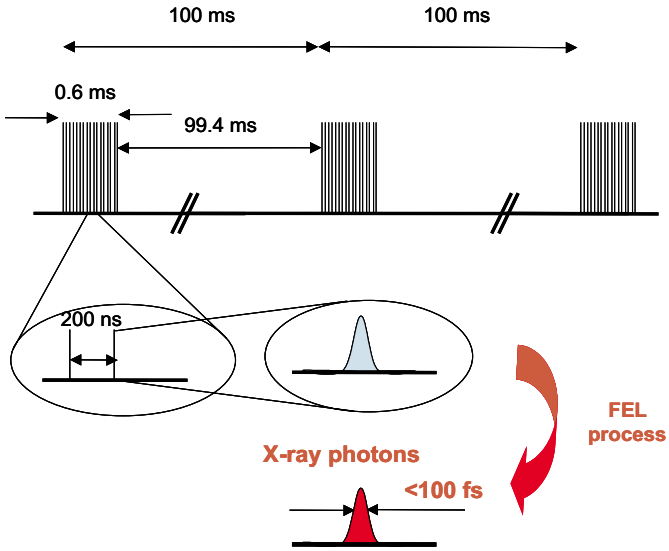

Figure 4: Time structure of the European XFEL.

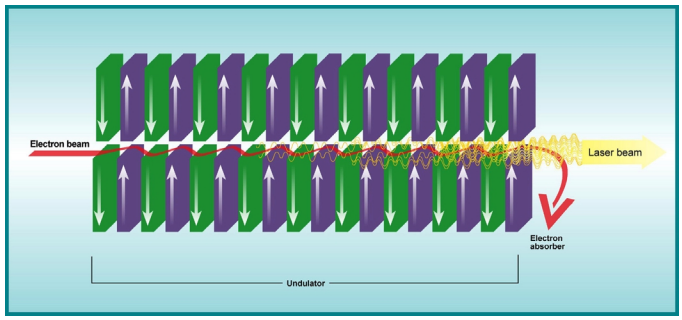

Figure 5: Schematic illustrating working principle of a SASE undulator.

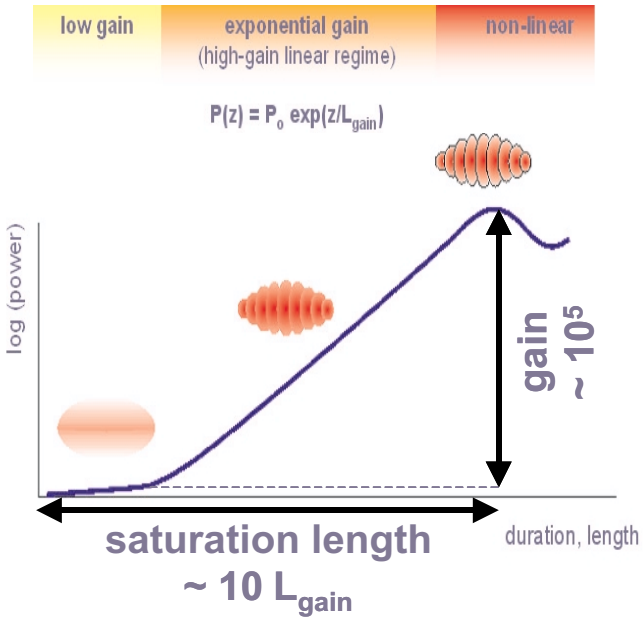

Figure 6: Power (intensity) of the FEL radiation versus undulator length.

B. SASE Undulator Sources and Beamlines

Accelerated charges emit electromagnetic waves, which is one of the predictions of Maxwell's equations. Thus deflected (i.e. transversely accelerated) electrons emit synchrotron radiation, which has a continuous spectrum. To achieve a coherent, monochromatic beam, the emitted radiation has to interact with the emitting media – the electron beam packet in this case – on a periodical basis. But unlike in a dye laser (which in most other respects will serve as a good analogue) there is no "resonator" for X-rays and the real periodic structure of an undulator magnet has to be used: When an electron bunch enters an undulator, it will spontaneously emit photons of several wavelengths when passing the first "bents" of an undulator. Given the right direction and wavelength of this *random seed*, such photons from the rear part of the electron bunch can interact with photons further ahead in the bunch passing the next "bent" of the undulator and stimulate them to coherently emit synchrotron radiation at the same wavelength as the initial photon (c.f. fig. 5). Thus the power and intensity of the photon beam will exponentially rise along the length of the undulator, while the energy loss of the emitting electrons will cause a *microbunch* structure of the electron packet. This *microbunching* will ultimately saturate the intensity of the radiation and terminate the self-amplification process, since the limit for the electron density in the microbunches is reached after a certain number of undulator periods. This is illustrated in fig. 6. Obviously not only the fundamental wavelength, defined by electron energy, the magnetic field and period length of the undulator, but also higher harmonics of it are amplified.

In the first phase of the European XFEL three SASE undulators will be installed, which will provide photons with energies between 0.25 keV and 12.4 keV for nine photon beamlines. These undulators consist of $\approx 5\mathrm{m}$ long sections and are based on the design of those used in FLASH. Each SASE undulator consists of 21 to 42 of these modules, separated by beam focusing elements like quadrupole magnets. Table 1 summarises the properties and scientific applications of the individual undulator sources.

III. Experiments

A. XPCS - X-Ray Photon Correlation Spectroscopy

X-ray photon correlation spectroscopy probes the dynamical properties of condensed matter, like e.g. phase transitions, protein folding, viscoelastic flow, crystalline phase transitions or domain switching. These are accessed in the time domain by looking at the normalised autocorrelation function:

[b]

Table 1: Properties and scientific applications of the 3 XFEL SASE undulator sources.

Beamline	X-ray features	Proposed instruments
SASE 1	$\approx 12\text{keV}$ High coherence High flux 3^{rd} harmonic	PCS 1 X-ray Photon Correlation Spectroscopy FDE 1 - Femtosecond Diffraction Experiments SPB 1 - Single Particles and Biomolecules
SASE 2	$3.1 \ldots 12.4\text{keV}$ High coherence High flux	CXI 1 - Coherent X-ray Imaging HED 2 - High Energy Density XAS 2 - X-ray Absorption Spectroscopy
SASE 3	$0.25 \ldots 3.1\text{keV}$ High coherence High flux 3^{rd} harmonic	HED 1 - High Energy Density SQS 1 - Small Quantum Systems XAS 1 - X-ray Absorption Spectroscopy SQS 1 - Small Quantum Systems PCS 2 - X-ray Photon Correlation Spectroscopy CXI 1 - Coherent X-ray Imaging

$$g(t) = \frac{\langle n(t)n(t+\tau)\rangle}{\langle n\rangle^2}, \tag{1}$$

which can be calculated from the speckle pattern of the photons scattered by the material. However, in sequential XPCS setups τ in eq. 1 is limited by the rate of the synchrotron source or the detector, as fig. 7 shows. Thus only phenomena with time constants larger than τ can be investigated.

1) XPCS splitted-pulse technique

To overcome this limitation and investigate phenomena occurring on time scales close to the length of the X-ray pulse, the so-called splitted-pulse technique can be employed. It is illustrated in fig. 8 and does no longer permit the calculation of the autocorrelation function, since the result is only a single image. However the change of contrast with the pulse delay can be used to calculate the temporal evolution of the system.

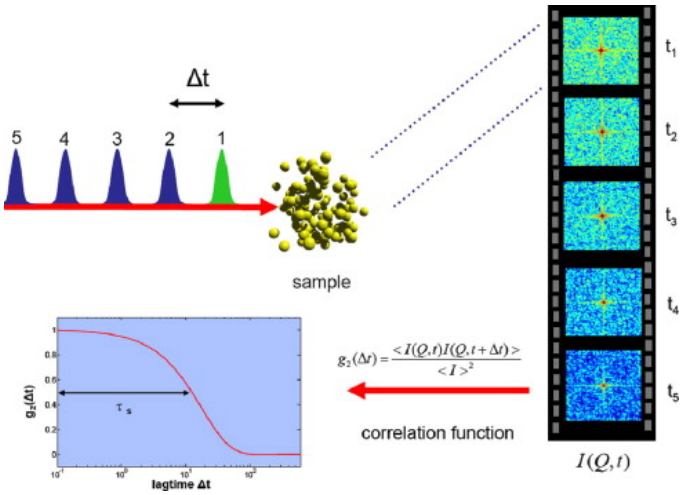

Figure 7: Illustration of the XPCS sequential technique (taken from [2]).

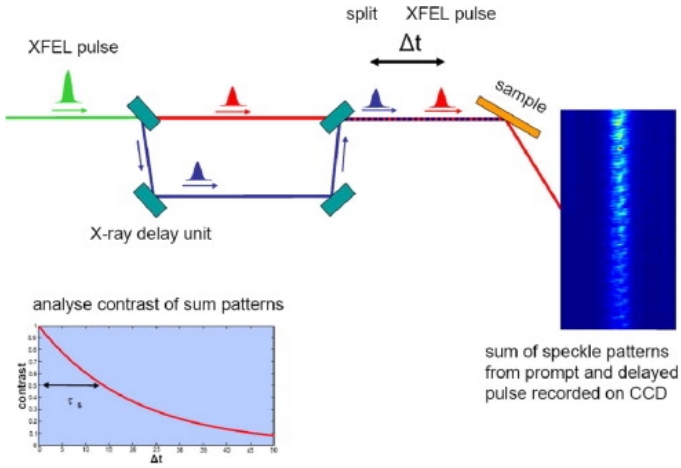

Figure 8: Illustration of the XPCS splitted-pulse technique (taken from [2]).

1) Pump-Probe Experiments

This is a third class of XPCS experiment, which can only be used to investigate phenomena, which are triggered by an external pump pulse. This is usually an electromagnetic signal like switching on a magnetic field or a laser pulse. As fig. 9 shows, the autocorrelation function $g(t)$ can now be calculated from the delay between pump and probe pulse. Also in this case the length of the synchrotron pulse defines a lower limit for τ. The long readout time of conventional imaging detectors (in the region of several ms) and the x-ray pulse rate of synchrotrons set the lower limits for the time scale of phenomena accessible with XPCS sequential techniques to the regime of milliseconds. Circumventing these limits with spitted-pulse or pump-probe techniques, which is not always possible, moves this limit to fractions of a microsecond, since the length of a synchrotron pulse is typically $\approx 200\,\text{ps}$ long. The European XFEL will -together with suitable detectors- lower the limits for phenomena accessible to sequential XPCS techniques to the µs regime, due to the 200 ns bunch spacing. In case of splitted-pulse and pump-probe experiments an even bigger improvement is achieved: The XFEL pulse length of $\leq 100\,\text{fs}$ will move the limits to the

picosecond regime, such that the dynamics of most chemical reactions become accessible.

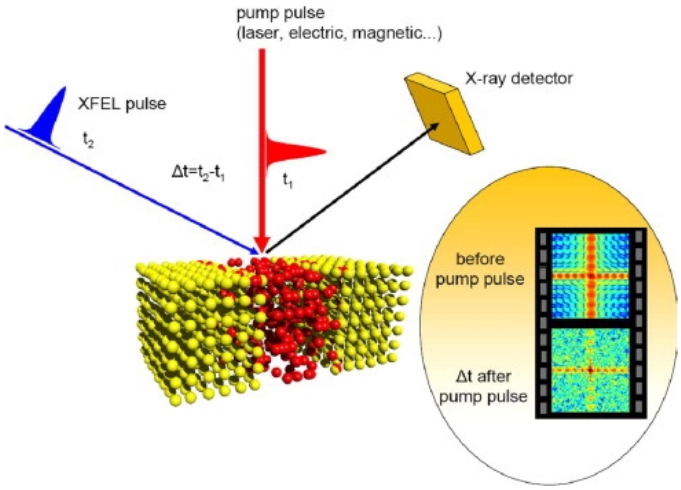

Figure 9: Illustration of the XPCS pump-probe technique (taken from [2]).

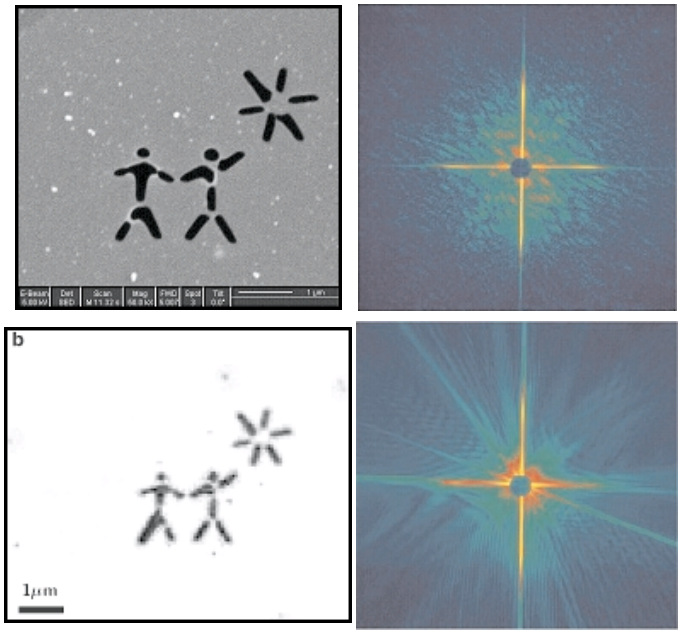

Figure 10: XCDI of a picture etched into a 35 nm thick layer of silicon nitride [3].
Top left: TEM image of the sample.
Top right: Diffraction pattern from the first FLASH UV pulse.
Bottom left: Image reconstructed from the diffraction pattern without using information about the sample.
Bottom right: Diffraction pattern from a second FLASH pulse proving the destruction of the sample.

B. XCDI - Coherent Diffraction Imaging

This technique can be used at the European XFEL to investigate the structure of cells, viruses, biomolecules and other nano-objects. These structures were only accessible if these objects could be forced to form regular structures, as it is well known from protein crystallography. However, it should also be possible to image single molecules and nano-objects, if the very low crossection can be overcome with a sufficiently high flux of coherent photons. But such a high photon density will also ionize the sample and cause it to disintegrate in a coulomb explosion. At FLASH it was shown, that this process takes longer than ≈ 100 fs as shown in fig. 10, and that it is possible to reconstruct the object by means of a phase retrieval algorithm, without using any information about the original. Given the higher intensity and photon energy, it will be possible to XCDI to Biomolecules and similar objects to reconstruct their structure, as illustrated in fig. 11.

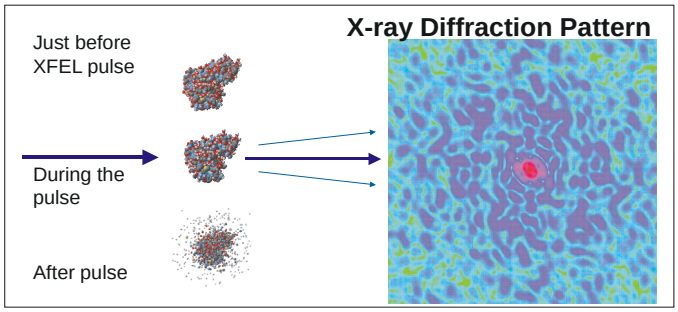

Figure 11: Schematic principle of XCDI with single biomolecules [3].

IV. 2D Area Detectors

The diffraction patterns from such experiments will be recorded with pixel detectors, which not only have to satisfy the experiment type specific requirements given in tab. 2, but also have to comply with the European XFEL's time structure shown in fig. 4. Further challenges arise from the high photon flux: The innermost pixel regions will be exposed up to 10^4 photons per shot. Thus the detectors will accumulate up to 1GGy of TID within 3 years. The resulting effects and radiation damage in silicon sensors is investigated in a common research project for all XFEL detector developments. Despite the shielding by the sensor, up to 10 % of the deposited dose will be accumulated by the readout asics beneath the sensors, which requires the use of radiation tolerant deep submicron CMOS technology and/or radiation hard layout techniques. Another issue related to the high photon flux is the charge density ($\approx 10^8$ electron-hole pairs) generated by up to 10^5 photons incident on a 10 µm $\times$ 10 µm area in some experiments. Here the charge of the electrons will shield the drift field and a deterioration of the spatial resolution by *diffusion before drift* – the so-called *charge explosion* – is expected. In turn its investigation within a research project for all XFEL detectors has been established. Despite these obstacles, the DEPFET-APS LPD and AGIPD consortia took up to the challenge to build pixel area detectors for the European XFEL. The basic concepts and parameters of these detectors are summarised in tab. 3.

[t]

Table 2: Detector requirements of different XFEL experimental techniques.

	PPnX	PPX	CDI	SPI	XPCS
E [keV]	$6 \ldots 15$	12	$0.8 \ldots 12$	12.4	$6 \ldots 15$
$\Delta E/E$	No	No	No	No	No
QE	≥ 0.8	≥ 0.8	≥ 0.8	≥ 0.8	≥ 0.8
Rad Tol	10^{16}ph	10^{16}ph	2×10^{16}ph	2×10^{15}ph	2×10^{14}ph
Size	200 deg	120 deg	120 deg	120 deg	0.2 deg
Pixel	7 mrad	100 µm	0.1 mrad	0.5 mrad	4 mrad
# pixels	500×500	3k × 3k	20k × 20k	4k × 4k	1k × 1k
tiling	$< 20\%$	$< 10\%$	See text		$< 20\%$
L Rate	5×10^4	3×10^6	10^5	10^4	10^3
G Rate	3×10^7	10^7	10^7	10^7	10^6
Timing	10 Hz	10 Hz	5 MHz	10 Hz	5 MHz
Flat F	1%	1%	1%	1%	1%
Dark C	< 1ph	< 1ph	< 1ph	< 1ph	< 1ph
R Noise	< 1ph	< 1ph	< 1ph	< 1ph	< 1ph
Linearity	1%	1%	1%	1%	1%
PSF	1 pixel	100 µm	1 pixel	1 pixel	1 pixel
Lag	10^{-3}	10^{-3}	7×10^{-5}	10^{-3}	10^{-3}
Vacuum	No	No	Yes	Yes	No
Other	Hole	Hole			Hole

Table 3: Concepts of the three different XFEL pixel detector projects.

	DEPFET-APS	LPD	HPAD
# of pixels	1 k × 1 k	1 k × 1 k	1 k × 1 k
Pixel size	200 µm × 200 µm	500 µm × 500 µm	200 µm × 200 µm
Sensor	DEPFET array	Si-pixel	Si-pixel
Dynamic range	$\geq 10^4$ ph	2×10^4 ph (10^5 ph)	$\geq 2 \times 10^4$ ph
Noise	$\approx 15 \times 10^{-3}$ ph ≈ 50e	≈ 0.21 ph (≈ 0.93 ph) ≈ 700 e (≈ 3100 e)	$\approx 45 \times 10^{-3}$ ph ≈ 150 e
Concept	DEPFET nonlinear gain compression Per-pixel ADC	Multiple gain paths On-chip ADC	Adaptive gain switching (preset gain option)
Storage	8bit DRAM	3-fold analogue	2 bit digital + analogue
Storage depth	≥ 256	512	≥ 200
Challenges	Linearity & calibration In-pixel ADC DRAM refresh Power budget Pixel area	Preamplifier: noise, dynamic range & PSRR Analogue storage	Dynamic gain switching Charge injection Analogue storage Pixel area
	Radiation hardness		

A. *Large Pixel Detector (LPD)*

This detector to be built by a consortium consisting of STFC and the University of Glasgow [4] will feature a shingled arrangement of the detector tiles with pixels of 500 µm × 500 µm – thus the name. The overall layout of the detector is depicted in fig. 13, while a single sensor module is depicted in fig. **??**.

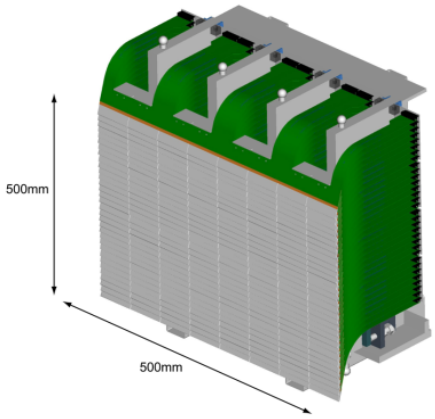

Figure 12: Overall layout of the LPD detector.

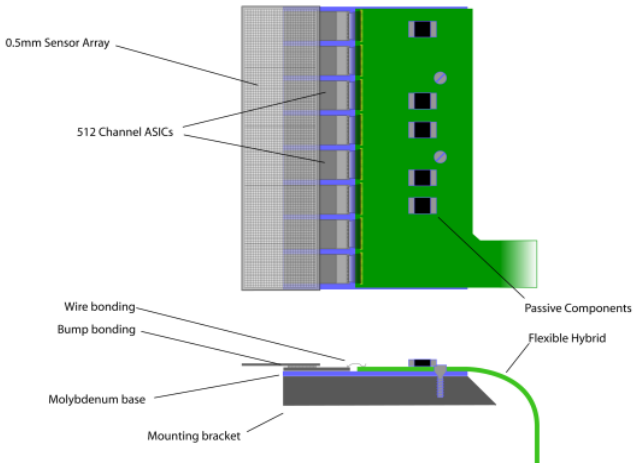

Figure 13: Sensor module of the LPD detector.

The sensor of each module is divided in 128×32 pixels, read out by 8 ASICs with 512 channels each. The basic concept of this readout ASIC is a threefold readout pipeline fed by the same preamplifier, but with different gains. This concept, which is depicted in fig. 14, has been successfully used for the readout of the high dynamic range in several calorimeters at CERN. Single photon sensitivity can be achieved with 20 pF feedback capacitance, as the noise simulation in fig. 15 shows.

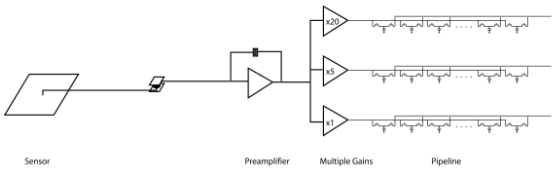

Figure 14: Threefold gain path of the LPD detector readout.

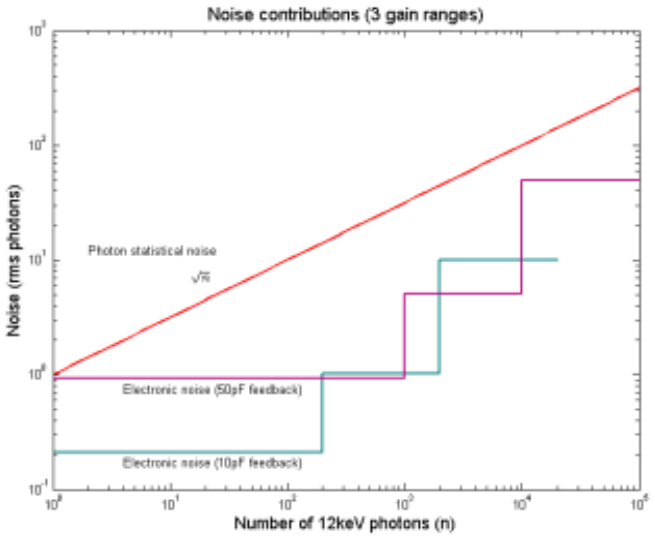

Figure 15: Noise simulation of the LPD detector readout ASIC.

B. *DEPFET Active Pixel Sensor (DEPFET-APS)*

This detector is proposed by a consortium of MPI Halbleiterlabor, Munich, DESY, the Universities of Bergamo, Heidelberg and Siegen, and the Polytecnico di Milano [5]. Unlike the other two detectors, it will make use of active sensor arrays based on the DEPFET principle. As shown in fig. **??** a potential well underneath the gate of the DEPFET will collect the charges generated by ionising radiation in the bulk of the transistor. The drain-source current in this transistor is than not only modulated by the gate voltage, but also by the field induced by the charges in the potential well. In case of the sensors used for the DEPFET-APS detector, this potential well extends underneath the source for higher energy levels. Small amounts of charge will therefore be trapped in the minimum of the well and fully contribute to the steering effect. If more charge is accumulated, some part of the charge is stored under the source and thus will not contribute to the steering effect: The characteristic of the DEPFET becomes nonlinear and a compression effect is achieved. The readout of a DEPFET sensor can be done e.g. by biasing it with a current source and reading the voltage at the source – the so-called source follower readout. The subsequent datapath is depicted in fig. 17: It consists of a preamplifier, a filter, sample and hold and an 8-bit ADC stage writing to DRAM based buffer memory inside each pixel. The DEPFET sensors are divided into 128×512 DEPFET pixels of 200 µm × 200 µm. The final detector will feature 1 megapixel and will consist of a planar arrangement of 8×2 sensors.

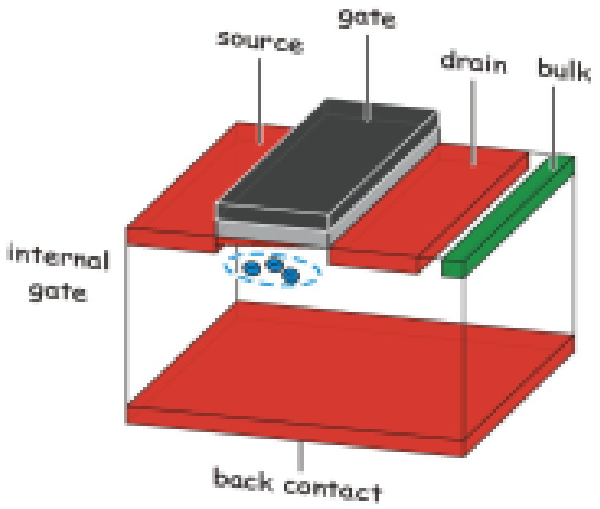

Figure 16: Principle of a DEPFET sensor: The radiation-induced charge accumulated in the potential well below the gate will modulate the DEPFET's drain current.

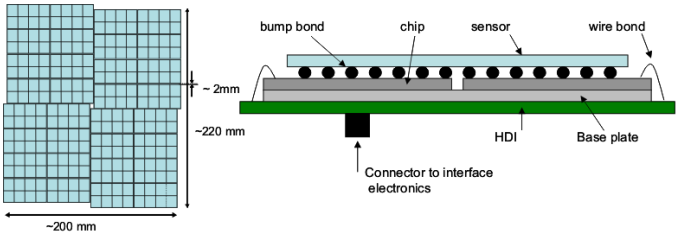

Figure 18: Left: Sensor arrangement of the AGIPD detector. Right: Crossection of a AGIPD sensor module.

To cover the required dynamic range of 2×10^5 photons, while providing single photon sensitivity, the charge sensitive preamplifier of each pixel features an adaptive gain: If the amplifier output exceeds a certain level, a discriminator is triggered, causing an additional feedback capacitor to be connected in parallel with the original one. By this the gain is lowered from $1/C_1$ to $1/(C_1 + C_2)$ without loosing any of the already integrated charge.

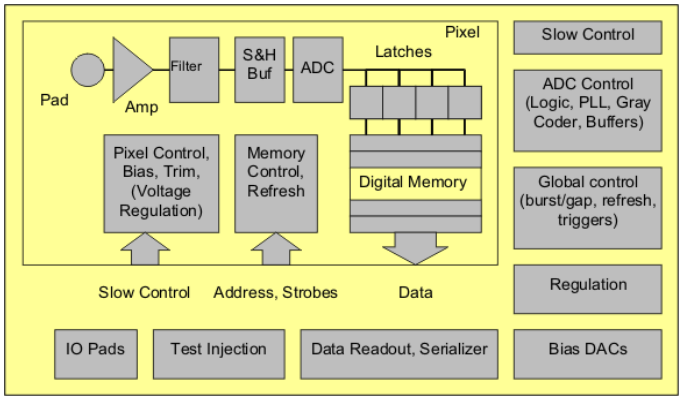

Figure 17: Block schematic of the DEPFET-APS readout chip.

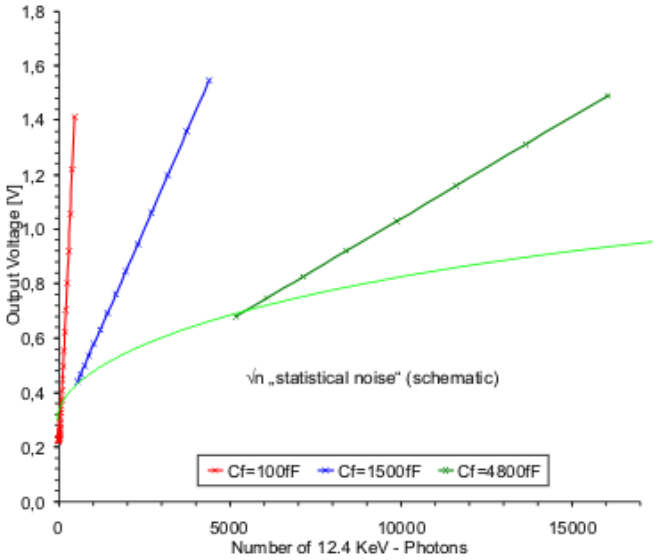

Figure 19: Simulation of the AGIPD adaptive gain characteristic. The parabolic curve visualises the statistical fluctuation of the registered signal. electronic noise should be well below this limit, while higher sensitivity than given by this curve will only register statistical fluctuations.

C. Adaptive Gain Integrating Pixel Detector (AGIPD)

This is a segmented planar 1 megapixel detector built by a consortium of the Universities of Bonn and Hamburg, DESY and PSI [6]. The detector will be constructed from 4 radialy movable quadrants, such that the size of the central hole for the direct beam can be adjusted. Each quadrant consists of 2×44 sensors of 256×128 pixels each. The sensors are bump-bonded to 2×4 readout chips of 64×64 channels, which are mounted on an high-density interconnect flexprint, as shown in fig. 18.

The AGIPD pixels will feature three different gain settings (as shown in fig. 19) and their selection has to be propagated along with the analogue information. The latter will be recorded by double correlated sampling in an capacitor array, as is the gain setting by encoding it to easily distinguishable analogue levels, as depicted in the pixel schematic in fig. 20. By this the same readout path can be used for analogue and digital information. However, since the readout of 200 frames from the chip will take several 10 ms, signal droop caused by leakage currents in switches and capacitors becomes an issue and all analogue information is read before the encoded gain settings. The AGIPD consortium has identified this problem and is investigating leak-

age currents in the chosen 130 nm (IBM cmrf8sf DM) CMOS technology, also under the influence of temperature and radiation.

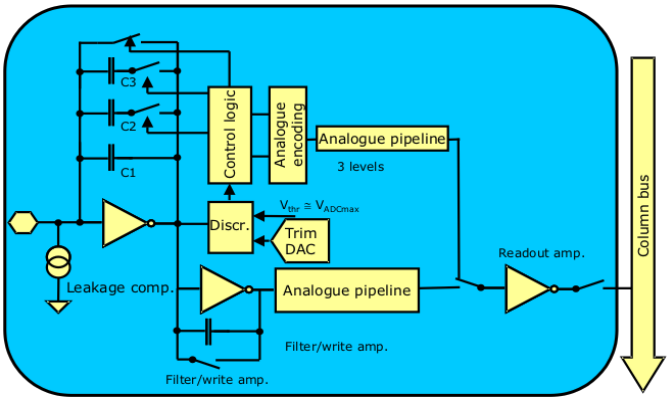

Figure 20: Schematic of a AGIPD readout chip pixel.

V. Summary

- Signing of the Contract for the XFEL GmbH (company) scheduled for the begin of 2009,
  the start of civil construction is scheduled for Feb. 2009
- Accelerator:
  Prototype XFEL modules, similar to those of FLASH/TTF, exist and were successfully tested.
- Undulators:
  These modules are based on those used in FLASH, also here XFEL prototypes exist
- 2D area detectors
  - 3 projects took up the challenge
  - Individual solutions to the dynamic range challenge were elaborated
  - Same CMOS process for readout ASICs was selected by all 3 consortia.
- Ongoing studies on possible obstacles
  - Charge Explosion
  - Radiation hardness (test chips by LPD and AGIPD exist.)
- First pixels in silicon scheduled for 2009
- Full area detectors planned for 2012

References

[1] M. Altarelli et al., The European X-Ray Free-Electron Laser Technical Design Report, DESY 2006-097, ISBN 978-3-935702-17-1

[2] G.Grü bel et al., XPCS at the European X-ray free electron laser facility, *Nucl. Instr. Meth. Phys. Res.* B 262 (2007) 357367

[3] Pictures courtesy of H. Chapman, J. Hajdu et al.

[4] M. French et al. Large Pixel Array Detector proposal

[5] M. Porro et al. DEPFET Adaptive Pixel Sensor proposal

[6] H. Graafsma et al. The Analogue Pipe-Line Hybrid Pixel Array Detector proposal